MHD Stellar and Disk Winds: Application to Planetary Nebulae

Eric G. Blackman[1,2], Adam Frank[1], and Carl Welch[1]
1. Department of Physics & Astronomy, University of Rochester, Rochester, NY 14627
2. ITP, University of California, Santa Barbara, CA 93106

(accepted to ApJ)

arXiv:astro-ph/0005288v3 18 Aug 2000

Abstract

MHD winds can emanate from both stars and surrounding disks. When the two systems are coupled by accretion, it is of interest to know how much wind power is available and which (if either) of the two rotators dominates that power. We investigate this in the context of multi-polar planetary nebulae (PNe) and proto-planetary nebulae (PPNe), for which recent observations have revealed the need for a wind power source in excess of that available from radiation driving, and a possible need for magnetic shaping. We calculate the MHD wind power from a coupled disk and star, where the former results from binary disruption. The resulting wind powers depend only on the accretion rate and stellar properties. We find that if the stellar envelope were initially slowly rotating, the disk wind would dominate throughout the evolution. If the envelope of the star were rapidly rotating, the stellar wind could initially be of comparable power to the disk wind until the stellar wind carries away the star's angular momentum. Since an initially rapidly rotating star can have its spin and magnetic axes misaligned to the disk, multi-polar outflows can result from this disk wind system. For times greater than a spin-down time, the post-AGB stellar wind is slaved to the disk for both slow and rapid initial spin cases and the disk wind luminosity dominates. We find a reasonably large parameter space where a hybrid star+disk MHD driven wind is plausible and where both or either can account for PPNe and PNe powers. We also speculate on the morphologies which may emerge from the coupled system. The coupled winds might help explain the shapes of a number of remarkable multi-shell or multi-polar nebulae. Magnetic activity such as X-ray flares may be associated with the both central star and the disk and would be a valuable diagnostic for the dynamical role of MHD processes in PNe.

Subject headings: jets and outflows; accretion, accretion disks; planetary nebulae: general; ISM: magnetic fields: MHD; stars: AGB and post-AGB

1. Introduction

Planetary Nebulae (PNe) and proto-Planetary Nebulae (PPNe) are believed to be the penultimate evolutionary stage of low and intermediate mass stars (zero age main sequence mass range $0.8M_{\odot} < M_{zams} \leq 5M_{\odot}$). PNe appear on the sky as expanding ionized plasma clouds surrounding a hot central star. As the resolution of ground based telescopes increased, the "typical" shape of a PN went from spherical (Osterbrock 1972) to elliptical and/or bipolar (Balick 1987). More recently, deeper and higher resolution studies (particularly those with the HST) have shown many PNe with narrow collimated features that are better described as *jets* than *bipolar lobes*. In some cases the jets appear as extremely well collimated bipolar outflows: M2-9 (Balick 2000): Hen-401 (Sahai 2000), AFGL 2688 (The Egg) (Sahai *et al.*1998). In other cases they appear as FLIERS (Fast Low-Ionization Emission Regions), a single knot expanding away from a (usually) elliptical nebula. In addition to the presence of jets it also appears that many PNe show evidence for multi-shell structures or multi-polarity. In these objects two nested pairs of bipolar lobes appear. In multi-shell structures the lobes are aligned along the same axis of symmetry (Hb 12: Welch *et al.*1999) while multi-polar cases show different orientations for the inner and outer lobes (M2-46: Manchado *et al.*2000).

While considerable progress has been made in understanding the hydrodynamics or magneto-hydrodynamics of shaping bipolar lobes (see Frank 1999 for a review), the origin of jets, point symmetry and multi-polar outflows in PNe poses fundamental challenges for theory.

The basic hydrodynamics of bipolar outflows can be described by the classic Generalized Interacting Stellar Winds (GISW) model (Kwok *et al.*1978, Kahn & West 1986, Balick 1987, Icke 1988). In this scenario a slow (10 km s^{-1}), dense (10^{-4} M$_{\odot}$ yr^{-1}) toroidal wind expelled during the AGB is followed by a fast (1000 km s^{-1}), tenuous (10^{-7} M$_{\odot}$ yr^{-1}) wind driven off the contracting proto-white dwarf during the PNe phase. The GISW model can explain bipolar morphologies and even jets. Point-symmetry and multi-polar bubbles however, do not fall easily into line with the concept of a large-scale collimating torus.

Models invoking a toroidal magnetic field embedded in a normal radiation driven stellar wind have recently shown some promise. This so-called *Magnetized Wind Bubble (MWB)* model was first proposed by (Chevalier & Luo 1994) and has been studied numerically by (Rozyczka & Franco 1996) and (García-Segura *et al.*1999). In these models the field at the star is dipolar but assumes a toroidal topology due to rapid stellar rotation. Collimation is not activated until the wind passes through the inner shock. Then hoop stresses associated with the toroidal field dominate over isotropic gas pressure forces and material is drawn towards the axis producing a collimated flow. This mechanism has been shown capable

of producing a wide variety of outflow morphologies including well collimated jets. When precession of the magnetic axis is included in fully 3-D simulations, the MWB model is capable of recovering point-symmetric morphologies as well (García-Segura 1997). It is noteworthy that the wind in these models differs substantially from standard MHD driven winds in disk and stellar wind contexts, and the fundamental issue of collimation before the wind-wind interaction remains to be addressed. In addition it is not clear that such models can be applied to multi-polar bubbles due to the difference in collimation orientations.

Finally neither the GISW or MWB models fully address the origin of the wind. This becomes a critical issue when one is dealing with Proto-Planetary Nebulae (PPNe). There is growing evidence suggesting that the PN shaping process begins in the PPN phase via well collimated jets (Sahai & Trauger 1998). The creation of fast ($V > 100$ km/s) high mass loss rate ($\dot{M} > 10^{-6}$ M$_\odot$ yr^{-1}) winds during these early phases when the star is an F or G type is not easily explained via classic line driven wind theory as the available power is insufficient (Alcolea et al. 2000). Thus for PPN, theorists face a dilemma similar to the problem of YSO outflows in that they must explain *both* wind acceleration and collimation (Pudritz 1991, Königl & Ruden 1993, Shu *et al.*1994).

The above considerations motivate further study of magnetized wind models for the launching and collimation of outflows from PN. In particular, the basic question of the available MHD wind power is important to address.

Magnetically driven outflows are a leading paradigm for a ubiquity of source classes in nature. This includes such contexts as protostellar jets (c.f. Smith 1998; Frank 1999 for reviews), the Solar wind (c.f. Parker 1979), jets of Galactic accretors (c.f. Mirabel and Rodriguez 1999), active galactic nuclei (c.f. Ferrari 1998; Blandford 2000 for reviews), and gamma-ray bursts (e.g. Usov 1992; Duncan & Thomspon 1992; Blackman et al. 1996; Meszaros & Rees 1997; Ruderman et al. 2000). While the parameter regimes are varied and the extent and nature of collimation, particle acceleration, and radiation process are different in the different settings, an underlying principle remains: magnetic fields can act as a drive belt between gravity and energy deposition at large radii, extracting the rotational energy of the rotator into an outflow. We note that the potential for accretion disks to exist in PPN systems has been raised (Morris 1987; Soker & Livio 1994; Reyes-Ruiz & Lopez 1999).

In the case of PN, as in other star-disk or compact object-disk systems, the magnetically driven outflows can in principle emanate from both the central object or the disk. Because the relative collimation and power evolution of the disk and stellar winds can be different, it may not be unreasonable to see outflows of different character coexisting in the same object. In order to investigate this properly however, it is necessary to allow that the disk

and star are coupled and this requires a model for the disk evolution.

A careful investigation of the relevant disk formation is presented in Reyes-Ruiz & Lopez (1999). The disk in this study forms when a binary system undergoes common envelope evolution. The ejection of the envelope involves transfer of angular momentum from the secondary to the envelope after which the secondary loses enough angular momentum to fall to a separation such that it can fill its Roche lobe and form the disk. Reyes-Ruiz & Lopez (1999) discuss a number of important constraints on the constituents and properties of binaries which lead to disk formation. The most likely system turns out to be an evolved AGB star with mass $2.5 < M_{agb}/M_{\odot} < 5$ for the primary, with a secondary of mass $\lesssim 0.08 M_{\odot}$ and with an initial binary separation of $> 50 - 100 R_{\odot}$ (Iben 1991). The AGB star will shed 80% of its mass during the common envelope ejection, leaving a post AGB stellar core of Mass M_c surrounded by a thin residual convective shell.

The time scale for the disk to move to its inner inner radius is of order or shorter than the viscous time scale. Even for systems whose initial outer radii are of order $100 R_{\odot}$, the relevant time scale would be no more than a few years. Since the disk would form only after the period of common envelope ejection, $<$ 1yr, we would expect the disk and the stellar shell to form concurrently within a time of order a few years. Because the relevant stellar field will be exposed once the envelope ejection occurs, and because any stellar dynamo growth time in the disk (discussed later) is less than 1 year, we suggest the rotating stellar shell and disk could both support co-operative jets at a time coincident within about a year after the disk forms. This represents the initial time appearing in our calculations.

In section 2, we determine the MHD wind power from PPN stars and disks. This requires a calculation of the expected field strength in the disk and a model of how the accretion affects the stellar field, the stellar spin, and the disk inner radius. We study the cases for which the stellar shell is initially rapidly or slowly rotating, and calculate the maximum disk and stellar magnetic wind powers for each case. In section 3 we discuss the observational implications of the results of the power calculation and speculate on the magnetic shaping. We summarize and conclude in section 4.

2. Winds from Disks and Stars

There are many models of magnetic jet production and collimation in the literature. The extent and explicit details of collimation are perhaps less agreed upon than the principles of launching. Magnetic launching mechanisms can be divided into two basic classes, "spring" mechanisms (Uchida & Shibata 1985; Contopoulos 1995 Lynden-Bell 1996)

and "fling" mechanisms (Blandford & Payne 1982; Lovelace et al. 1987). In the former class of models, the initial driving force is a magnetic spring, i.e. the magnetic field energy density is of order the kinetic energy density in the disk and the outflow is driven by toroidal field pressure. In the fling mechanism, the initial driving is centrifugal along poloidal field lines. Higher up in the corona the wind becomes magnetically driven. In this study we compute the total available magnetic luminosity L_m from the disk and central star. The magnetic luminosity provides an upper limit to the associated wind kinetic luminosity. The L_m is the integral of the Poynting flux over the surface area of the rotator. We thus have

$$L_w \sim \dot{M}_w V_w^2 \sim \epsilon L_m = \epsilon \int (\mathbf{E} \times \mathbf{B}) \cdot d\mathbf{S} \sim \epsilon \int_{R_i}^{R_o} (\Omega R) B_p B_\phi R dR, \tag{1}$$

where ϵ is an efficiency, and B_ϕ and B_p are the toroidal and poloidal field respectively, Ω and R are the rotational frequency and radius of the magnetized wind source, $\dot{M}_m$ is the wind outflow rate, and V_w is the wind outflow speed. In what follows we discuss this equation in the context of PPN disks and post AGB stars. For all cases of interest, for disks the integrand falls off fast enough such that the inner radius matters most. Thus for disks we have

$$L_{dw} \sim \epsilon_d L_{dm} \sim \epsilon_d B_p(R_i) B_\phi(R_i) \Omega_d(R_i) R_i^3, \tag{2}$$

where Ω_d is the disk angular speed L_{dm} is the available magnetic luminosity associated with the disk, and ϵ_d is the unknown efficiency factor. For stars, we have

$$L_{sw} \sim \epsilon_s L_{sm} \sim B_p(R_*) B_\phi(R_*) \Omega_*(R_*) R_*^3, \tag{3}$$

where Ω_* is the angular speed of the stellar surface in which the field lines are anchored, L_{sm} is the available magnetic luminosity associated with the star, and ϵ_s is the stellar wind efficiency factor. The above disk and stellar wind luminosities are not independent. The poloidal and toroidal fields are coupled through differential rotation in both the disk and star, and the angular velocity of the star may depend on the accretion. In addition, the inner radius of the disk depends on the stellar magnetic field. Thus (2) and (3) are very much interdependent.

We now proceed to solve for the coupling relations and consider the stellar and disk MHD wind luminosities for two cases:

- The star is initially a strongly magnetized rotator independent of the accretion.
- The star is initially a slow rotator but is spun up by the disk accretion.

As we will see, the evolution in both cases depends on estimates of the disk and star magnetic fields. We must also solve for the disk inner radius, and the stellar surface angular speed evolution.

2.1. Magnetic Field of Disk

If the jet/wind is due to a magnetic field in the disk, this field must be produced in situ for the PN case. This is because the companion star, the progenitor of the disk, would have to be a brown dwarf or a Jupiter type planet (Reyes-Ruiz & Lopez 1999) which typically would only have fields of order or less than 10G. Even a field several orders of magnitude larger would be far too small to have any influence on the disk, which forms from shredding this mass, if the disk field were only that resulting from flux freezing. We estimate the field strength roughly from dynamo or turbulent amplification in the disk. An alternative dynamo approach to ours is given by Reyes-Ruiz & Stepinski (1995).

For an accretion disk whose angular momentum is transported by a magneto-shearing instability (c.f. Balbus-Hawley 1991, 1998), the time scale for growth of unstable modes and the time scale for the largest eddy turnover time are both approximately equal to the rotation time scale. Very roughly, the eddy turnover time can be written as L/v_T where v_T is the dominant turbulent velocity and L is the dominant correlation scale. We can estimate the strength of the mean magnetic field by first estimating the total magnetic energy. Using the Shakura-Sunyaev (1973) viscosity prescription

$$\nu = \alpha_{ss} c_s H \sim v_T^2/\Omega, \tag{4}$$

where α_{ss}, c_s, H and L/v_T are the disk viscosity parameter, the sound speed, the scale height and the dominant eddy turnover time respectively. Using the fact that turbulent stretching leads to $v_A \sim v_T$, where v_A is the Alfvén speed (ignoring a possible factor of $\sqrt{2}$ on v_T, e.g. Balbus & Hawley 1998) , and $\Omega R = c_s R/H$ for a thin accretion disk, we then have straight away

$$v_A^2 = \alpha_{ss} c_s^2. \tag{5}$$

When modeled as a mean-field $\alpha_d - \Omega$ dynamo (c.f. Parker 1979; Reyes-Ruiz & Stepinski 1995; Blackman 2000), it can be shown that due to the differential shear, the mean toroidal field exceeds the saturated mean poloidal field strength in the disk by a factor of H/L. From (4) and (5) we have $L \sim \alpha_{ss}^{1/2} H$ and thus

$$B_p \sim \alpha_{ss}^{1/2} B_\phi. \tag{6}$$

Whether this relation holds true in the base of the disk corona where the jet would launch is unclear, but since the field in the corona is no greater than the field in the disk, the overall disk mean field provides a good upper limit at least to the total mean field energy density. Note that the total mean stress $\langle B_\phi B_p \rangle = \langle \overline{B}_\phi \overline{B}_p \rangle + \langle b_\phi b_p \rangle$, where the second term is a correlation of fluctuating fields. Actually, both of these terms can drive a wind. Exploring this point is outside the scope of the present paper, and here we simply stick with

the standard approach (e.g. Blandford & Payne 1982) where the large scale fields drive the wind. Thus we ignore the $\langle b_\phi b_p \rangle$ term.

The upper limit of the mean field is of order the random field, so from (5) we have, for the dominant disk field component,

$$B_\phi^2 \sim 4\pi\rho_d\alpha_{ss}c_s^2. \tag{7}$$

From the mass continuity equation of the disk we have,

$$\rho_d = \dot{M}_a/(4v_R\pi HR), \tag{8}$$

where v_R is the radial infall speed. For (thin or ADAF) disks

$$v_R \sim \alpha_{ss}c_sH/R \sim \alpha_{ss}v_k(H/R)^2, \tag{9}$$

where $v_k^2 = GM/R$, the Keplerian speed. Then using (7) and (8) and (9), we have

$$B_\phi B_p = \alpha_{ss}^{1/2}B_\phi^2 = \frac{\alpha_{ss}^{1/2}(R/H)v_k(R)\dot{M}_a}{R^2}. \tag{10}$$

This expression can be used to estimate either the magnetic field strength or Maxwell stress avialable in the disk for launching a wind.

2.2. Magnetic field of the stellar shell

The relevant stellar field is the field at the anchoring radius of the post AGB star from which the wind emanates. Observational interpretation suggests that the common envelope ejection, which would precede disk formation, removes $\sim 80\%$ of an initially $\sim 3M_\odot$ star (Schönberner 1993). Convective stellar models for a $3M_\odot$ star (Kawalar, private communication 2000) then tell us that outer layer will have a convective shell containing a mass of order $0.01M_\odot$. We allow for a distinction between the core of the star M_c and the mass in which the field is anchored, M_*. The latter is likely to be equal to the core mass if the field is generated by an AGB interface dynamo (Blackman et al. 2000), but if the field were somehow anchored only in the thin shell, M_* might be $<< M_c$.

Since the convective shell is likely to be differentially rotating with respect to the core we assume that the shear rate is of order the anchoring material's angular speed, Ω_*. The shear will stretch a dynamo produced poloidal field linearly in time. The linear streching could operate coherently over a vertical diffusion time $\tau_D \sim R_*^2/\eta_T$, where $\eta_T \sim Lv_T$ is the turbulent diffision coefficient for turbulent velocity v_T and scale L. (This would need to

be calculated for specific interface dynamo models, c.f. Parker 1993; Markiel & Thomas 1999; Blackman et al 2000). Using numbers from Kawaler (private communication 2000), the diffusion time could be of order a few times the convective overturn time for the largest eddies in the post-AGB star, about 0.05yr. In any case, for linear growth of the toroidal field, the toroidal and poloidal fields are then related by

$$B_{\phi *} \sim B_{p*} \Omega_* \tau_D, \tag{11}$$

which follows from the magnetic induction equation. Although the poloidal field B_{p*} will likely also depend on Ω_*, it will also depend on other properties of the turbulence and the mechanism of field origin (c.f. Parker 1979, 1993; Pascoli 1997; Soker 1998; Markiel & Thomas 1999; Blackman et al. 2000). For an initial treatment of the problem, we simply consider B_{p*} as an input condition.

2.3. Disk inner radius

Now that we have the stellar magnetic field, we can calculate the disk inner radius. Related calculations were performed by Ghosh & Lamb (1978) and Ostriker & Shu (1995). We estimate the inner radius by balancing the infall ram pressure from the disk with the magnetic pressure of the star. For the infall velocity we use the free fall velocity, as that corresponds to the field strength at which the disk must absolutely truncate. Thus our calculation represents a lower limit on the inner radius. Note for example that when the Alfvén speed in the disk, using the stellar field strength, equals the sound speed there, magneto-shearing instabilities will be shut off. At this field strength the nature of the angular momentum transport must change (to e.g. global modes, B.Chandran, E.Ostriker, 2000 personal communication). We assume that a suitable change occurs and thus still use the larger Keplerian speed for the balance below.

Using the r^{-3} dependence for a dipole field and considering only the values at the equator $r = R$, we have

$$\frac{1}{4\pi} B_*^2 \left(\frac{R_*}{R_i} \right)^6 \simeq \rho_{d,i} v_{k,i}^2, \tag{12}$$

where $v_{k,i}$ is the Keplerian ($\sim$ free-fall) speed at R_i. Note that when $\Omega_* \tau_D \gtrsim 1$, $B_*^2 \sim B_{\phi *}^2$, otherwise $B_*^2 \sim B_{p*}^2$. This is important because the angular speed couples in the former case but not in the latter.

The next step is to use the mass continuity equation (8) for R_i. The result is

$$R_i = B_{p*}^{4/7} (1 + \Omega_*^2 \tau_D^2)^{2/7} \alpha_{ss}^{2/7} (H_i/R_i)^{6/7} R_*^{12/7} (GM_c)^{-1/7} \dot{M}_a^{-2/7}. \tag{13}$$

The inner radius will be time dependent because of the time dependent accretion rate and angular speed of the anchoring material. We now compute the evolution of this angular speed.

2.4. Angular Speed of the Star

The disk and stellar wind luminosities depend on the angular velocity Ω_* of the stellar material where the field is anchored. As shown above, Ω_* is one factor which determines the magnetic pressure of the star, and thus R_i. For small τ_D, Ω_* decouples from R_i.

If material is accreting onto the star from the disk at rates based on the disk formation models of Reyes-Ruiz and Lopez (1999), then

$$\dot{M}_a \sim 6 \times 10^{22} \left(\frac{t}{1\mathrm{yr}} \right)^{-5/4} \mathrm{g/s}, \tag{14}$$

and there may be some contribution to the rotation from the accreted material. There are many complications in this accretion process. Here we simply assume that the material imparts its angular momentum to the shell (e.g. via the magnetic field) as it accretes. We also assume that the accreted material does not change the thickness of the star. The rotation speed of the relevant stellar envelope is then determined by balancing the angular momentum gained from the accretion with that lost from the MHD stellar wind. We have the following approximate equation

$$M_* R_*^2 \frac{d\Omega_*}{dt} = -\dot{M}_a \Omega_* R_*^2 + \dot{M}_a \Omega_{k,i} R_i^2 - B_{p*}^2 \Omega_* R_*^3 \tau_D. \tag{15}$$

where $\Omega_{k,i}$ is the Keplerian angular speed at the disk inner edge, and we have assumed a constant R_*. The last term on the right hand side is due to the magnetic torque applied by the wind ($\propto B_{p*} B_{\phi*}$). This equation applies when R_i corresponds to a radius at which the disk is spinning faster than field lines of the star at that radius. Thus it is assumed that the disk accretion can spin up the stellar convective envelope. There exists a regime in which the star spins fast enough to disrupt the disk, and angular momentum of the star is lost to the disk. We do not consider that regime. Note further that if R_i were greater than the radius at which the co-rotation speed exceeded the Keplerian speed of the star, there would be no accretion (Armitage & Clarke 1996).

Re-arranging, and expanding the Keplerian term, we have

$$\frac{d\Omega_*}{dt} + \Omega_* (\dot{M}_a / M_* + B_{p*}^2 R_* \tau_D / M_*) \simeq \frac{(GM_c)^{1/2} \dot{M}_a R_i^{1/2}}{R_*^2 M_*}. \tag{16}$$

In the simple limit of no disk, only the 1st and 3rd terms of (16) would contribute and the solution would be

$$\Omega_* = \Omega_{*0} e^{-t/t_m}, \tag{17}$$

where we define the magnetic spin-down time scale t_m

$$t_m \equiv \frac{M_*}{B_{p*}^2 R_* \tau_D}. \tag{18}$$

This quantity is the spin-down time from MHD powered rotational energy loss. For typical parameters,

$$t_m \sim 50 \left(\frac{M_*}{M_\odot}\right) \left(\frac{B_{p*}}{10\mathrm{kG}}\right)^{-2} \left(\frac{R_*}{10^{11}\mathrm{cm}}\right)^{-1} \left(\frac{\tau_D}{10^5\mathrm{sec}}\right)^{-1} \mathrm{yr} \tag{19}$$

As we shall see there are two regimes of interest to pursue in analytic approximation depending on whether t/t_m is large or small.

For the kind of disks considered here, the second term in (16) can be ignored compared with the third. Also, for the maximum accretion rates we consider (*i.e.* $\sim 10^{-3} M_\odot \mathrm{yr})(t/1\mathrm{yr})^{-5/4}$, a mass shell of 0.01 $M_\odot$ will at most have a 30% gain in mass over the lifetime, because of the form of the time dependence, so we can assume M_* is a constant after the 1 year initial system formation period. The ODE can then be solved by standard integrating factor techniques, and is in fact analogous to an RL circuit. We find

$$\Omega_* = CExp\left[-\int^t \frac{dt'}{t_m}\right] + Exp\left[-\int^t \frac{dt'}{t_m}\right] \times \int^t Exp\left[\int^t \frac{dt}{t_m}\right] q(t')dt' \tag{20}$$

where we define

$$q(t) \equiv \frac{(GM_c)^{1/2} \dot{M}_a(t) R_i^{1/2}(t)}{R_*^2 M_*}. \tag{21}$$

Note again that we do not consider the solution before $t = 1\mathrm{yr}$ when the accretion disk is still forming. For the approximate early time solution, $t/1\mathrm{yr} < t/t_m < 1$, we set the exponentials equal to 1. The result (after the 1 yr disk formation grace period) is then

$$\Omega_*(t) \simeq \Omega_{*0} + \omega_0 \left(1 - \left(\tfrac{t}{1\mathrm{yr}}\right)^{-1/14}\right), \tag{22}$$

where

$$\omega_o = \frac{3 \times 10^8 (GM_c)^{1/2} \dot{M}_{a0} R_{i0}^{1/2}}{R_*^2 M_*}, \tag{23}$$

and where the subscript 0 indicates the quantity at its initial time ($t = 1$yr). We have ignored the time dependence in R_i from Ω_*, while including the implicit time dependence from $\dot{M}_a$. This is a good approximation for this regime because $R_i^{1/2}$ depends on $\Omega_*^{2/7}\dot{M}_a^{-1/7}$. Note that expression (22) allows us to define the difference between initially fast ($\Omega_{*0} > \omega_0$) and slow ($\Omega_{*0} < \omega_0$) stellar rotation.

When $t/t_m > 1$ the exponential in (20) begins to evolve quickly compared to the power law decay of the $\dot{M}_a R_i^{1/2}$ factor inside the last integral. Factoring this out and noting that the product of integrals in this last term then cancel, we have

$$\Omega_*(t) \sim q(t)t_m + (K - q(t)t_m)\, e^{(-t/t_m)}, \tag{24}$$

where $K = e\Omega_*(t_m) + q(t_m)t_m(1-e)$. For large times $(t/t_m) > 1$, the first term on the right of (24) dominates and we have

$$\Omega_*(t) \simeq q(t)t_m = \frac{(GM_c)^{1/2}\dot{M}_a R_i^{1/2}}{B_{p*}^2 R_*^3 \tau_D} = \alpha_{ss}^{1/7}\frac{(GM_c)^{3/7}\dot{M}_a^{6/7}(H/R)^{3/7}}{B_{p*}^{12/7}R_*^{15/7}\tau_D} \text{ (for } \Omega_*\tau_D < 1)$$
$$\alpha_{ss}^{1/5}\frac{(GM_c)^{3/5}\dot{M}_a^{6/5}(H/R)^{3/5}}{B_{p*}^{12/5}R_*^{3}\tau_D} \text{ (for } \Omega_*\tau_D > 1), \tag{25}$$

where the latter represents the case for which R_i depends on Ω_* from (13). Note that the equations of (25) should be used only when it produces a value below the corresponding escape speed.

2.5. Disk Wind Luminosities

Plugging (10) into (2), we have

$$L_{dw} = \dot{M}_{dw}V_{dw}^2 = \epsilon_d\alpha_{ss}^{1/2}\int B_\phi^2\Omega_k R^2 dR \sim \epsilon_d\alpha_{ss}^{1/2}\dot{M}_a(R_i/H_i)GM_c/R_i, \tag{26}$$

where $\dot{M}_{dw}$ indicates the outflow rate from the disk wind and V_{dw} is the disk wind outflow speed. We now consider several cases which involve using the appropriate value of R_i from section 2.3 in (26), then using the appropriate solution for Ω_* from section 2.4 in (13) for R_i. We will also use (14) for $\dot{M}_a$.

We first consider the case of slow stellar rotation ($\Omega_{*0} < \omega_0$). The maximally luminous case will have the smallest disk inner radius. For a given poloidal field, the toroidal stellar field will be weakest for slowly rotating stars as per our discussion above, so in this case the disk inner radius will be the smallest. When R_i as calculated in (13) satisfies $R_i \leq R_*$, we

use $R_i = R_*$ and the disk luminosity is given by

$$L_{dw} \simeq \frac{\epsilon_d \alpha_{ss}^{1/2} G M_c \dot{M}_a}{R_*} \left(\frac{R_*}{H_i}\right) \sim 10^{37} \frac{\epsilon_d \alpha_{ss,-2}^{1/2} \dot{M}_{a0,22} M_{c,1}}{R_{*,11}} \left(\frac{t}{1\mathrm{yr}}\right)^{-5/4} \left(\frac{R_*/H_i}{10}\right) \mathrm{erg/s}. \quad (27)$$

In this, and the expressions which follow, we scale α_{ss} to 0.01, magnetic fields to 10^4 G, radii to 10^{11} cm, diffusion times to 10^5 yr, stellar core masses to 1 $M_\odot$, stellar shell masses to 10^{-2} $M_\odot$, angular speeds to 10^{-4} Hz and mass loss rates to 10^{22}g s^{-1}. These scalings are indicated by the subscripts.

We now consider the case of an initially rapidly spinning star. The disk and star are strongly coupled through R_i and we must consider the different temporal regimes relative to the ratios t/t_m and $\Omega_* \tau_D$. When $t < t_m$ the first term on the right hand side of (22) dominates. Then using (13) for $\Omega_* \tau_D > 1$, we have

$$L_{dw} \simeq \frac{\epsilon_d \alpha_{ss}^{\frac{3}{14}} (G M_c)^{\frac{8}{7}} \dot{M}_a^{\frac{9}{7}}}{B_{p*}^{\frac{4}{7}} \tau_D^{4/7} \Omega_*^{\frac{4}{7}} R_*^{\frac{12}{7}}} \left(\frac{R_i}{H_i}\right)^{13/7} \sim 7 \times 10^{37} \frac{\epsilon_d \alpha_{ss,-2}^{\frac{3}{14}} M_{c,1}^{\frac{8}{7}} \dot{M}_{a0,22}^{\frac{9}{7}}}{\left(B_{p*,4} \tau_{D,5} \Omega_{*0,-4}\right)^{\frac{4}{7}} R_{*,11}^{\frac{12}{7}}} \left(\frac{t}{1\mathrm{yr}}\right)^{\frac{-45}{28}} \left(\frac{R_i/H_i}{10}\right)^{\frac{13}{7}} \frac{\mathrm{erg}}{\mathrm{s}}. \quad (28)$$

For $t > t_m$, using (13) (under the assumption that $B_{\phi *} \gtrsim B_{p*}$, or equivalently $\Omega_* \tau_D > 1$), and (25) in combination with (26), we have

$$L_{dw} \simeq \epsilon_d \alpha_{ss}^{\frac{1}{70}} (G M_c)^{\frac{4}{5}} \dot{M}_a^{\frac{3}{5}} B_{p*}^{\frac{4}{5}} \left(\frac{R_i}{H_i}\right)^{\frac{11}{5}} \sim 10^{38} \epsilon_d \alpha_{ss,-2}^{\frac{1}{70}} M_{c,1}^{\frac{4}{5}} \dot{M}_{a0,22}^{\frac{3}{5}} B_{p*,4}^{\frac{4}{5}} \left(\frac{t}{50\mathrm{yr}}\right)^{\frac{-3}{4}} \left(\frac{R_i/H_i}{10}\right)^{\frac{11}{5}} \frac{\mathrm{erg}}{\mathrm{s}} \quad (29)$$

In the limit that $\Omega_* \tau_D < 1$ or $B_{p*} > B_{\phi *}$, from (13) we obtain instead,

$$L_{dw} \sim \frac{\epsilon_d \alpha_{ss}^{\frac{1}{14}} (G M_c)^{\frac{8}{7}} \dot{M}_a^{\frac{9}{7}}}{B_{p*}^{\frac{4}{7}} R_*^{\frac{12}{7}}} \left(\frac{R_i}{H_i}\right)^{\frac{13}{7}} \sim 7 \times 10^{35} \frac{\epsilon_d \alpha_{ss,-2}^{\frac{1}{14}} M_{c,1}^{\frac{8}{7}} \dot{M}_{a0,22}^{\frac{9}{7}}}{B_{p*,4}^{\frac{4}{7}} R_{*,11}^{\frac{12}{7}}} \left(\frac{t}{50\mathrm{yr}}\right)^{\frac{-45}{28}} \left(\frac{R_i/H_i}{10}\right)^{\frac{13}{7}} \frac{\mathrm{erg}}{\mathrm{s}}. \quad (30)$$

For the characteristic numbers used, (29) does not apply because a check of $\Omega_* \tau_D$ from (25) reveals that $\Omega_* \tau_D < 1$ for $t > t_m$ for our parameter regime.

The above formalism is valid when the magnetic luminosity is $\lesssim$ the accretion luminosity $G \dot{M}_* M_c / R_i$. If the magnetic luminosity exceeds the disk luminosity, then the disk structure would be disrupted and the formalism would have to be revisited.

2.6. Stellar wind luminosities

The stellar wind luminosity is given by (3). We note again the hidden dependence of the field on the rotational velocity. If a dynamo generates the stellar field, then both B_p

and B_ϕ can depend on Ω_*. For example the rotation would be required to generate the pseudoscalar helicity that sustains a steady field in dynamo models. Also, the toroidal field may induce poloidal field by springing outward. More subtle dependences should be considered in future work, but the important point here is the recognition of some dependence on the rotation, and thus on the supply of angular momentum from the disk. Here we simply assume that the poloidal field of the star is kept at a constant value either by a dynamo or by buoyancy of toroidal field, while the toroidal field depends linearly on the rotational speed as implied by growth from shear. In this case, equation (3) gives

$$L_{sw} \sim \epsilon_s B_{*p} B_{*\phi} \Omega_* R_*^3 \sim B_{p*}^2 \Omega_*^2 \tau_D R_*^3. \tag{31}$$

We now consider the same temporal regimes for the stellar wind power that were examined for the disk wind. For a rapidly rotating star in the $t < t_m$ regime, the first term on the right hand side of (22) is dominant and from (31) we then have,

$$L_{sw} \simeq \epsilon_s B_{p*}^2 \Omega_{*0}^2 \tau_D R_*^3 = 10^{38} \epsilon_s B_{p*,4}^2 \Omega_{*0,-4}^2 \tau_{D,5} R_{*,11}^3 \text{ erg/s}. \tag{32}$$

For a very slowly rotating star in the $t < t_m$ regime, the second term on the right of (22) is dominant. The spin evolves to within a factor of 1/10 of ω_o after a few years. In this case Ω_* is such that R_i from (13) is less than R_* so we take $R_i = R_*$. The stellar rotation rate and wind power thus approach

$$\Omega_* \sim (3 \times 10^7) \sqrt{\frac{G M_c \dot{M}_{a0}^2}{R_*^3 M_*^2}}, \tag{33}$$

and

$$L_{sw} \sim 3 \times 10^{31} \epsilon_s \frac{B_{p*,4}^2 \tau_{D,5} M_{c,1} \dot{M}_{a0,22}^2}{M_{*,1}^2} \text{ erg/s}. \tag{34}$$

respectively. The slow time evolution in (22), which results in the approximation that the angular speed and luminosity are constant in (33) and (34), reflects the fact that during this period, the angular momentum gain from accreted material and the loss of angular momentum from the wind nearly balance.

For $t > t_m$, but for $\Omega_* \tau_D > 1$, using (25) and (13) with (31), we have

$$L_{sw} \sim \frac{\epsilon_s \alpha_{ss}^{\frac{2}{5}} (G M_c)^{\frac{6}{5}} \dot{M}_a^{\frac{12}{5}}}{B_{p*}^{14/5} R_*^3 \tau_D} \left(\frac{H_i}{R_i}\right)^{\frac{6}{5}} = 10^{28} \frac{\epsilon_s \alpha_{ss,-2}^{\frac{2}{5}} M_{c,1}^{\frac{6}{5}} \dot{M}_{a0,22}^{\frac{12}{5}}}{B_{p*,4}^{\frac{14}{5}} R_{*,11}^3 \tau_{D,5}} \left(\frac{t}{50\text{yr}}\right)^{-3} \left(\frac{R_i/H_i}{10}\right)^{\frac{-6}{5}} \frac{\text{erg}}{\text{s}}. \tag{35}$$

For $t > t_m$, when $\Omega_* \tau_D < 1$, we have instead

$$L_{sw} \sim \frac{\epsilon_s \alpha_{ss}^{\frac{2}{7}} (G M_c)^{\frac{6}{7}} \dot{M}_a^{\frac{12}{7}}}{B_{p*}^{\frac{10}{7}} R_*^{\frac{9}{7}} \tau_D} \left(\frac{H_i}{R_i}\right)^{\frac{6}{7}} = 10^{30} \frac{\epsilon_s \alpha_{ss,-2}^{2/7} M_{c,1}^{\frac{6}{7}} \dot{M}_{a0,22}^{\frac{12}{7}}}{B_{p*,4}^{\frac{10}{7}} R_{*,11}^{\frac{9}{7}} \tau_{D,5}} \left(\frac{t}{50\text{yr}}\right)^{\frac{-15}{7}} \left(\frac{R_i/H_i}{10}\right)^{\frac{-6}{5}} \frac{\text{erg}}{\text{s}}, \tag{36}$$

which is larger in comparison to (35) because a smaller field means a slower decay of Ω_*. For the characteristic numbers used, $\Omega_*\tau_D$ from (25) satisfies $\Omega_*\tau_D < 1$ for $t > t_m$, as also mentioned above, so here only (36) would apply for our parameter regime and not (35).

2.7. Slow and Rapid Initial Stellar Rotation Cases

In fig 1 we show plots of the disk to stellar wind luminosity ratios using $\epsilon_s = \epsilon_d$ for two different stellar rotation regimes.

Slow Rotation: In fig 1a and 1b plots of L_{dw}/L_{sw} for the slow rotator case ($\Omega_{*0} < \omega_0$) are given. Fig 1a shows essentially the ratio of (27) to (34) and fig 1b shows the ratio (27) to (36). For both the $t << t_m$ and $t >> t_m$ regimes, the disk wind luminosity strongly dominates the stellar wind luminosity by orders of magnitude. This dominance decreases with time in the former regime and increases in the latter regime. However the main feature is that for the entire range, the disk wind dominates the stellar wind.

The star is therefore slaved to the disk throughout the evolution in this case. The stellar wind and spin axes are also slaved to those of the disk because the toroidal field is stretched perpendicularly to the axis of rotation and the wind emanates perpendicularly to the toroidal field. The disk and stellar winds would thus be coaxial, but the disk wind would strongly dominate.

Rapid Stellar Rotation: In fig 1c and 1d we present plots of L_{dw}/L_{sw} for the rapid rotator case ($\Omega_{*0} > \omega_0$). For $t < t_m$ the plot shows basically the ratio of (28) to (32) and for $t > t_m$ the plot shows the ratio of (30) to (36). For $t < t_m$, the stellar wind is comparable to, and even slightly dominates the disk wind luminosity for the parameters used, while for $t > t_m$ the disk wind dominates strongly. As in the slow rotator case, the disk wind domination decreases slowly for $t < t_m$ and increases for $t > t_m$.

Thus for the large Ω_{*0} case, with Ω_{*0} near maximal speeds, the stellar wind is independent of the disk until $t = t_m$. After this time its MHD wind luminosity is negligible compared to that of the disk. (If there were no disk at all, one would see only the rapid fall of of the stellar wind as in equation (17)). The initial independence of the star from the disk means that the axes of the two winds can be misaligned. The origin of the stellar spin and magnetic axes are decoupled since the spin axis of the disk is independently determined by the initial plane of the binary orbit. Thus the disk and stellar wind system can produce a multi-polar wind system of up to $\sim 10^{38}$erg/s, depending on the efficiency of conversion of rotational energy.

3. Discussion

Our results show that powerful magneto-centrifugal winds can be driven in PNe systems. In the context of accretion disks formed from the break-up of a secondary star in a binary system, these winds are time dependent and have a finite lifetime. Thus our results would predict that transient, magnetized outflows can be driven during the transition from AGB to PNe. Magneto-centrifugally driven winds potentially solve two problems which have emerged from PNe studies (Frank 2000). First, the large powers computed above can explain how strong winds can be driven independently of radiation line driving processes as required by observations in the PPNe phase (e.g. Alcolea et al 2000). Second, they may explain the high degree of collimation seen in some sources (e.g. Sahai & Trauger 1998), and multi-polar outflows when the disk and stellar winds are contemporaneous. Below we discuss these points further.

3.1. Accounting for the power of PN or PPN winds:

The calculations above show that magnetically driven winds can account for the large powers observed in PPNe. Alcolea et al. (2000) make the case that observations of PPNe are the best place to infer the required powers and shaping mechanisms of PNe. None of the 3 objects for which Alcolea et al. (2000) have measured kinetic ages (OH 231.8; M 1-92; M2-56) can be radiation driven at the PPNe stage. The required outflow powers range from 10^{35} erg/s to 10^{37}erg/s. The kinetic ages are fairly similar, ranging from 750 yr to 1800 yr. The radiation driving falls short of being able to provide the power by at least two orders of magnitude. The 9 objects for which Alcolea et. al (2000) have measured wind energies but not kinetic ages look reasonably similar in terms of radiation power and energetics. Since the kinetic ages for the few measured objects are not widely varying, it is likely that others in the population of 9 also probably require high outflow powers.

The powers computed in section 2 for MHD wind driving can be as high as 10^{38} erg/s for the parameters used. Such powers are therefore sufficient for PNe and PPNe. There is likely to be some efficiency factor with which the driving can take place, so to explain a 10^{37} erg/s wind, we would require an efficiency factor of $\epsilon \sim 10\%$. More study is needed to determine the ϵ factors dynamically.

For $t > t_m$, the disk wind power falls by two orders of magnitude or so, while the stellar MHD wind is of negligible power. The MHD disk wind could still supply e.g. $\sim 10^{36}$ ergs/s after ~ 50 yr, continuing to fall as $t^{1.6}$ from (30). Specific examples of kinetic powers required in this approximate range include Hb5 ($V_w \lesssim 400$ km/s and $\dot{M} \sim 6 \times 10^{-5} \dot{M}_\odot$/yr; [Corradi

& Schwarz 1995; Pishmish et al. 2000]) thus with a kinetic luminosity $L_w \lesssim 3.6 \times 10^{36}$erg/s; IC4406 ($V_w \sim 65$ km/s [Corradi al. 1997] and $\dot{M} \sim 10^{-4}\dot{M}_\odot$/yr [Sahai et al. 1991; Cox et al. 1991]) with $L_w \sim 2 \times 10^{35}$erg/s; M2-9 ($V_w \sim 46$ km/s [Solf 2000] and $\dot{M} \sim 4 \times 10^{-6}\dot{M}_\odot$/yr [Zweigle et al. 1997]) with $L_w \sim 5 \times 10^{33}$erg/s. Observations of NGC 3242, NGC 6828, NGC 7009, and NGC 7662 PNe (Balick et al. 1998; Dwarkadas & Balick 1998) are also consistent with $10^{33}\text{erg/s} \leq L_w \leq 10^{35}\text{erg/s}$.

In all cases, a dynamo in either a disk or the star or both may be responsible for the field driving the wind. Magnetic flaring and the production of hard coronal X-rays might then be expected in PPN engines. Observations with Chandra and other X-ray telescopes are therefore be highly desirable.

3.2. Accounting for the shapes of PN or PPN winds ?:

Given that the fields can power jets, they may also play a role in shaping them. One possible approach to MHD collimation in these sources is simulated in García-Segura et al. (1999). Since we have not yet dynamically calculated or simulated collimation mechanisms as applied to planetary nebulae the discussion that follows is speculative. The fact that the power of the disk and stellar winds can be comparable motivates us to proceed.

It is known that in the context of disks (e.g. Königl & Pudritz 2000 for review) and even in the context of stars (Tsinganos & Bogovalov 2000) that magnetic self collimation can be an important effect. The literature on collimation of disk winds is extensive. It is noteworthy that in emphasizing that fast rotating stellar magnetospheres can also collimate winds, Tsinganos & Bogovalov (2000) point out that such collimation from an underlying rotator will likely be effective when the quantity

$$Q = 0.12 \left(\frac{\psi}{\psi_\odot}\right) \left(\frac{\Omega}{\Omega_\odot}\right) \left(\frac{\dot{M}_w}{\dot{M}_\odot}\right)^{-1/2} \left(\frac{V_w}{V_\odot}\right)^{-3/2} \tag{37}$$

is greater than 1. Here ψ is the magnetic flux anchored on the rotator spinning at angular speed Ω, $\dot{M}_w$ is the outflow mass loss rate, V_w is the outflow speed, and these values are scaled to the respective values for the Sun, namely $V_\odot = 400$km/s, $\dot{M}_\odot = 1.6 \times 10^{12}$g/s, $\Omega_\odot = 3 \times 10^{-6}$/s and $\psi_\odot = 10^{22}$G-cm^2. We then have

$$Q/Q_\odot \simeq 4.2 \left(\frac{B_{*,4} R_{*,11}^2}{10^{26}\text{G} \cdot \text{cm}^2}\right) \left(\frac{\Omega_*}{10^{-4}/\text{s}}\right) \left(\frac{\dot{M}_{sw}}{6 \times 10^{21}\text{g/s}}\right)^{-1/2} \left(\frac{V_{sw}}{400\text{km/s}}\right)^{-3/2}, \tag{38}$$

where we have scaled to our fiducial post-AGB star parameters, taking the upper limit of the magnetic flux, and assuming a kinetic luminosity of the wind $L_{kin} \simeq \dot{M}_{sw} V_{sw}^2 \sim 10^{37}$erg/s.

We can see that $Q/Q_\odot$ can be greater than 1 for the chosen parameters, and thus collimation in excess of that for the solar wind can occur. If we instead use representative outflow parameters for later stages of PNe (e.g. Balick et al. 1998), such as $\dot{M} = 5 \times 10^{-7} M_\odot\,\mathrm{yr}^{-1}$ and $V = 200\,\mathrm{km\,s}^{-1}$), we find $Q/Q_\odot \gtrsim 100$ which implies significant collimation. In general, these estimates suggest that self-collimation of magnetized winds in PPNe and PNe might be possible without requiring shocks to aid in the process. The shock-aided approach has been studied in García-Segura et al. (1999). More study is warranted. The relative self-collimation of the disk wind and the stellar wind may be different for different systems. This needs to be studied.

Assuming collimation can ensue, the shape of any multi-polar magnetically driven outflow in our picture will also depend on the stellar spin down time scale t_m, and the time scale for the star to become a PN, $\equiv t_{PN}$. The ratio of t_m/t_{PN} will determine how much shaping will be controlled by the a combined star+disk wind. When $t_m/t_{PN} << 1$, the stellar wind is likely to provide micro-structures such as knots, bullets, or ansae in mature PNe. When $t_m/t_{PN} \gtrsim 1$ then structures such as multi-polar bubbles, which develop during the period when $L_{dw} \approx L_{sw}$, may leave a large enough imprint to survive into the PN phase.

Another important parameter is the ratio of the wind momentum densities, $p_{dw}/p_{sw} = \rho_{dw} V_{dw}/(\rho_{sw} V_{sw})$ where the ratio to be used here is that computed for each type of wind independent of the actual presence of the other. The momentum density depends on collimation and is thus a function of angle from a wind's axis. The terminal wind speed of material at a given radius from any wind axis depends on the details of the wind launching process but should be of order several times the the escape speed at the radius at which the field lines threading that radius are anchored (e.g. Königl & Pudritz 2000 for a review). The ratio p_{dw}/p_{sw} can in part determine the shape of the resulting observed outflow combination by determining which wind-driven "lobe" would extend farther when the two winds are superimposed. The difference in initial launch times of the two winds is also very important in determining the observed shapes.

For two concurrent winds satisfying $p_{dw}/p_{sw} > 1$ on average, and for which the star is rotating slowly ($\Omega_{*o} < \omega_o$), we might expect two nested aligned bipolar bubbles (as shown in Fig 2a) when the terminal speed of the stellar wind, calculated independently from the disk wind, is faster over most of the outflow cross-section. The stellar wind can sweep up disk material, but because of the lower overall momentum density, it cannot proceed as far in distance. An example of a PN with this shape is Hubble 12 (Welch *et al.*1999). When the stellar and disk magnetic and rotational axes are misaligned, a nested multi-polar bubble may emerge as shown in Fig 2c. A possible example of such an outflow is M2-46 (Manchado 2000) Please note again: Fig 2 represents cartoon speculations, not simulations.

When $p_{dw}/p_{sw} < 1$ and the star is rapidly rotating ($\Omega_{*o} > \omega_o$), the stellar wind could push ahead of the disk wind and may produce the features seen in e.g. NGC 7007 (Fig 2b, Balick *et al.*1998). In the case where the star is initially rapidly rotating and the stellar and disk axes are not aligned, then a second form of the nested multi-polar bubble may emerge as is shown in Fig 2d. An example of such an outflow may be He2-155 (Sahai 2000).

In the rapidly rotating case, the stellar wind remains more or less constant over a spin-down period while the disk wind falls. Thus we might expect the stellar wind to appear more or less continuous, whereas the disk wind could produce structures only of comparable luminosity to the stellar wind for the first several years. In this initial phase, antipodal knots amidst a continuous stellar wind might appear where the disk and stellar winds interact, or where the disk interacts with the ambient medium. Such processes might have been occurring in the Egg nebula (Jura et al. 2000).

Given that typical sound speeds for observed outflows are of order 20-30 km/s, while the wind velocities can be $>$ 100km/s, we can estimate the size of outflow structures compared with the distance from the star. For a hybrid disk-star outflow with strongest power phase lasting $\sim$ few years, but with an age or order hundreds of years, one should see knots (or shells depending on collimation) with a width of order 10^{16} cm. If the outflow velocity were 100 km/s, then the knot/shell distance from the central core would be ~ 5 times the shell thickness. Such features are seen in the Cat's Eye nebula (Miranda & Solf 1992)

Note that two interacting winds can lead to more than 2 multiple symmetry axis due to edge features. This and the features described above could also result from time dependent effects of separate interacting stellar winds or separate interacting disk winds where the star or disk is allowed to precess (e.g. Manchado et al. 1996). Precession would enable successive outbursts to be emitted on multiple axes. If there is precession, then one might see an additional point symmetry. These ideas may be applied to other coupled disk+star systems (Soker & Livio 1994, Mastrodemos & Morris 1998).

4. Summary and Conclusions

We have shown that MHD winds from either disks or post-AGB stars can comfortably power PNe outflows using reasonable estimates of stellar and disk field strengths and rotation parameters. The available MHD wind power turns out to be many orders of magnitude larger than that available for radiation/line driven outflows inferred from observations of PPNe (e.g Alcolea et al. 2000). Our study also highlights the importance

of understanding the interplay between disk winds and stellar winds in contributing to the diversity of observed multi-polar PNe morphologies.

We derived maximal disk and stellar MHD wind powers for a coupled disk-star system at times $t < t_m$, $t > t_m$, (where t_m is the stellar spin down time) and for fast and slow stellar rotators, $\Omega_*/\omega_0 <$ or > 1, and values of $\Omega_*\tau_D <$ or > 1. Our calculations take the initial time to be the onset of disk formation in a binary system from common envelope expulsion. The initial onset of the star and disk wind should be nearly contemporaneous. The layers of the star with the strong magnetic field that power the wind are only exposed after the common envelope is ejected, and the accretion disk forms within a year from the common envelope ejection.

The resulting luminosities for both winds depend only on the disk accretion rate and properties of the star. This is because the inner regions of the disk are the main contributor to the disk wind and the disk properties can be constrained using properties of magneto-shearing disks and the interaction with the star. We now summarize some numbers for the maximum wind powers:

* For $t << t_m$ and our choice of fiducial scalings, the maximum MHD luminosity of a stellar wind from an initially rapidly rotating post AGB star with field strengths consistent with those estimated for AGB dynamos of $\sim 10^4$ Gauss satisfies $L_{sw} \lesssim 10^{38}$ erg/s, and is approximately constant in time. The disk wind satisfies $L_{dw} \lesssim 7 \times 10^{37}(t/1\mathrm{yr})^{-1.6}$ as the accretion rate falls.

* After $t_m >> 50$yr, $L_{sw} \lesssim 10^{30}(t/50\mathrm{yr})^{2.1}$, and the disk wind power goes as $L_{dw} \lesssim 7 \times 10^{35}(t/50\mathrm{yr})^{-1.6}$.

* Whilst the dominance of disk vs. stellar wind depends on Ω_{*0} for $t << t_m$, for all $t >> t_m$, the disk wind always dominates, regardless of Ω_{*0}.

Since the MHD disk winds dominate the stellar winds for $t > t_m$ regardless of the initial stellar spin rate, the star is slaved to the disk in that regime. For $t < t_m$, the stellar wind power can equal or exceed that of the disk, and in this regime the stellar wind can emanate along a different symmetry axis than the disk wind. Multi-polar outflows can then be produced. For a rapidly rotating star, the stellar MHD wind power is steady for a time of order $t = t_m$, while the disk wind power falls rapidly. For $t > t_m$, the disk wind power falls less rapidly than the stellar wind power.

Generally, we would suggest that if a sustained MHD driven bipolar outflow extending to the core lasts for > 500 yr, the disk is dominant. The choice of scalings we use in the text were mainly to provide a general framework. The spin down time t_m could be longer than

our scale of 50 yr depending on radius and stellar convective diffusion time, (c.f. eqn (18)). Disk winds imply initial formation from a binary system. An initially rapidly rotating star would slow down rapidly by this later time, and would only be able to contribute significantly if its wind were radiatively driven at this stage. If a stellar wind operates powerfully during $t < t_m$ it means that the central star was initially rotating rapidly.

There is no guarantee that a binary system would form, or that the star would be initially rapidly rotating for every post AGB star. Thus for all systems with bipolar outflows, observations that can reveal the rotation rate of the central star, its magnetic field, or the presence of binary companions are ultimately essential for testing MHD disk/stellar wind paradigms. Further studies of the disk wind-stellar wind interplay are most certainly needed. Given the ubiquity of the accretion-central object-outflow connection throughout the universe the same kind of investigation may ultimately be important for other stellar and compact object accretion systems as well.

Acknowledgements: E.B. was supported in part by NSF grant PHY94-07194 at the ITP, and acknowledges support from a DOE Plasma Physics Junior Faculty Development Award. E.B. also thanks R. Krasnolpolsky, R. Blandford, B. Chandran, and E. Ostriker for discussions. Many thanks to G. García-Segura and M. Reyes-Ruiz for their careful readings which led to important changes.

Figure Captions

Figure 1: Plot of the MHD wind power ratio for the disk and star for four regimes with $\epsilon_s = \epsilon_d$: a) $t < t_m$ for the initially slowly rotating star b) $t > t_m$ for the initially slowly spinning star c) $t < t_m$ regime for initially fast rotating star. d) $t > t_m$ regime for initially fast rotating star. See text.

Figure 2: Cartoon representing our speculation on a possible correspondence between between HST PN images and multi-polar wind structures from the hybrid stellar-disk wind paradigm, for different initial stellar spins and thrust ratios Π_{dw}/Π_{sw} (see text). (Note that these are not simulations, but speculations.) a) top left: $\Omega_{*0} < \omega_0$ and $\Pi_{dw}/\Pi_{sw} > 1$ so star is slaved to disk and the only possibility is nested winds. Inset is PN Hubble 12 (Welch *et al.*1999). b) top right: $\Omega_{*0} < \omega_0$ and $\Pi_{dw}/\Pi_{sw} < 1$. Inset is NGC 7007 (Balick *et al.*1998). c) bottom left: $\Omega_{*0} > \omega_0$ and $\Pi_{dw}/\Pi_{sw} > 1$. Inset is M2-46 (Manchado *et al.*2000). d) bottom right: $\Omega_{*0} > \omega_0$ and $\Pi_{dw}/\Pi_{sw} < 1$. Inset is He2-155 (Sahai 2000). See text.

References

Alcolea J., Bujarrabal V., Castro-Carrizo A., Sánchez Contreras C., Neri R., Zweigle J. 2000, in *Asymmetrical Planetary Nebulae II: From Origins to Microstructures*, ASP Conference Series, Vol. 199. Edited by J. H. Kastner, N. Soker, and S. Rappaport, p347.

Armitage P.J. & Clarke C.J., 1996, MNRAS, 280, 458.

Balick, B. 1987, AJ, 94, 671

Balick B., in *Asymmetrical Planetary Nebuale II*, 2000 J.H. Kastner, N.Soker, & S. Rappaport eds., ASP Conf. Ser. Vol. 199., pg 41

Balick, B; Alexander, J., Hajian, A., Terzian, Y, Perinotto, M., Patriarchi, P., 1998, AJ, 116, 360

Balbus S.A. & Hawley J.F., 1991, ApJ , 376 214.

Balbus S.A. & Hawley J.F., 1998, Rev Mod Physics, 72 1.

Blackman E.G., Frank A., Markiel A., Thomas J., Van Horn H.M., 2000, submitted to Nature.

Blackman E.G., Yi I., Field G.B., 1996, ApJ, 473, L79.

Blackman E.G., 2000, ApJ 529, 138.

Blandford R.D. & Payne D.G. 1982, MNRAS, 199 883.

Blandford R.D., 2000, in "Proc of Discusison Meeting on Magnetic Activity in Stars, Discs and Quasars.", Ed. D. Lynden-Bell, E. R. Priest and N. O. Weiss. To appear in Phil. Trans. Roy. Soc. A

Chevalier, R., & Luo, D., 1994, ApJ, 421, 225

Contopoulos J., 1995, ApJ 450 616.

Corradi R.L.M. & Schwarz H.E., 1995, A&A 293 871.

Corradi R.L.M., Perinotto M., Schwarz H.E., Klaeskins J.F., 1997, A&A 322 975.

Cox, P., Huggins P. J., Bachiller R., Forveille T., 1991, A&A 250, 533.

Duncan R.C. & Thomson C., 1992, 392 L9

Dwarkadas V.V. & Balick B., ApJ, 1998, 497 267.

Ferrari A., 1998, ARAA, 36 539.

Frank A., 1999, New Ast. Rev., 43, p31.

Frank, A., in *Asymmetrical Planetary Nebuale II*, 2000 J.H. Kastner, N.Soker, & S. Rappaport eds., ASP Conf. Ser. Vol. 199., pg 225

García-Segura, G., 1997, ApJ, 489L, 189

García-Segura G., Langer N., Rozyczka, M., Franco J, 1999, ApJ 517 767.

Ghosh P.& Lamb F.K., 1978, ApJ 223, L83.

Iben I., 1991, ApJS 76, 55.

Icke, V., 1988, A&A, 202, 177

Jura M., Turner J. L., Van Dyk S., & Knapp G.R., 2000, ApJ, 528 L105.

Kahn, F. D., & West, K. A., 1985, MNRAS, 212, 837

Königl, A., & Ruden, S.P. 1993, in "Protostars and Planets III", ed. E.H. Levy & J.I. Lunine (University of Arizona Press), 641.

Königl, A.; Pudritz, R. E., 2000 in *Protostars and Planets IV*, eds Mannings, V., Boss, A.P., Russell, S. S.), (Tucson: University of Arizona Press; p. 759

Kwok, S., Purton, C., Fitzgerald, P. M., 1978, ApJ 219, L125

Lovelace R.V.E., Wang J.C.L., Sulkanen M.E., 1987 ApJ, 315 504.

Lynden-Bell D., 1996, MNRAS, 279 389.

Manchado A., Stanghellini L, Guerrero M.A., 1996, ApJ, 466 L95.

Manchado A., Villaver, E., Stranghelli, L., Guerrero, M., in *Asymmetrical Planetary Nebuale II*, 2000 J.H. Kastner, N.Soker, & S. Rappaport eds., ASP Conf. Ser. Vol. 199, pg 17

Mastrodemos, N., Morris, M., 1998, ApJ, 497, 303

Markiel J.A. & Thomas J.H., 1999, ApJ, 523 827.

Mészáros, P., & Rees, M.J. 1997, Ap.J. 482, L29

Miranda L.F. & Solf J., 1992, A&A 260 397.

Mirabel I.F. & Rodriguez L.F., 1999, ARAA, 37 409.

Morris, M. 1987, PASP, 99, 1115

Ostriker E.C. & Shu F.H., 1995, ApJ, 447, 813

Osterbrock, D., 1989, *Astrophysics of Gaseous Nebulae and Active Galactic Nuclei*, (University Science Books, CA)

Parker E.N., *Cosmical Magnetic Fields* (Oxford Univ Press: Oxford) 1979.

Parker E.N., 1993, ApJ, 408, 707.

Pascoli G., 1997, ApJ, 489, 946.

Pishmish P., Manteiga M., Mampaso Recio A., 2000 in *Asymmetrical Planetary Nebuale II*, 2000 J.H. Kastner, N.Soker, & S. Rappaport eds., ASP Conf. Ser. Vol. 199, pg 397.

Pudritz, R.E. 1991, in "The Physics of Star Formation and Early Stellar Evolution", eds. C.J. Lada and N.D. Kylafis, NATO ASI Series (Kluwer), pg 365.

Pelletier G. & Pudritz R.E., 1992, ApJ, 394 117.

Reyes-Ruiz M. & Lopez J.A., 1999, ApJ, 524 952.

Reyes-Ruiz M. & Stepinksi T.F., 1995, ApJ, 438 750.

Rozyczka, M., & Franco, J., 1996, ApJ, 469, 127

Ruderman M., Tao L., Kluzniak W., 2000, sub to ApJ, astro-ph/0003462

Sahai R., Wootten A., Schwarz H.E., Clegg R. E. S, 1991, A&A 251 560.

Sahai, R., & Trauger, J. T. 1998, AJ, 116, 1357

Sahai, Raghvendra; Trauger, John T., Watson, Alan M., Stapelfeldt, Karl R., Hester, J. J., Burrows, C. J., Ballister, G. E., Clarke, J. T., Crisp, D., Evans, R. W., Gallagher, J. S., III; Griffiths, R. E., Hoessel, J. G., Holtzman, J. A., Mould, J. R., Scowen, P. A., Westphal, J. A., 1998, ApJ, 493, 301

Sahai, R., in *Asymmetrical Planetary Nebuale II*, 2000 J.H. Kastner, N.Soker, & S. Rappaport eds., ASP Conf. Ser. Vol. 199, pg 209.

Schönberner D., 1993, in IAU Symp 155, *Planetary Nebulae* ed. R. Weinberger & A. Acker (Dordrecht: Kluwer) 415.

Shakura N.I. & Sunyaev R.A., 1973, A&A 24 337.

Shu F.H., Najita J., Ostriker E., Wilkin F., Ruden S., Lizano S., 1994, ApJ 429 781.

Smith M.D., 1998, Ap&SS 261 169.

Soker, N., Livio, M., 1994, ApJ, 421, 219

Soker N., 1998, MNRAS, 299, 1242.

Tsinganos, K., & Bogovalov S., 2000, Magnetic Collimation of Solar and Stellar Winds, *Astron. Astrophys.* in press.

Uchida Y. & Shibata K. 1985, PASJ, 37 31.

Usov V.V., 1992, Nature, 357, 472

Welch, C., Frank, A., Pipher, J., Forrest, W., Woodward, C., 1999, ApJ, 522L, 69

Zweigle J., Neri R., Bachiller R., Bujarrabal V., Grewing M., 1997, A&A, 324 624.

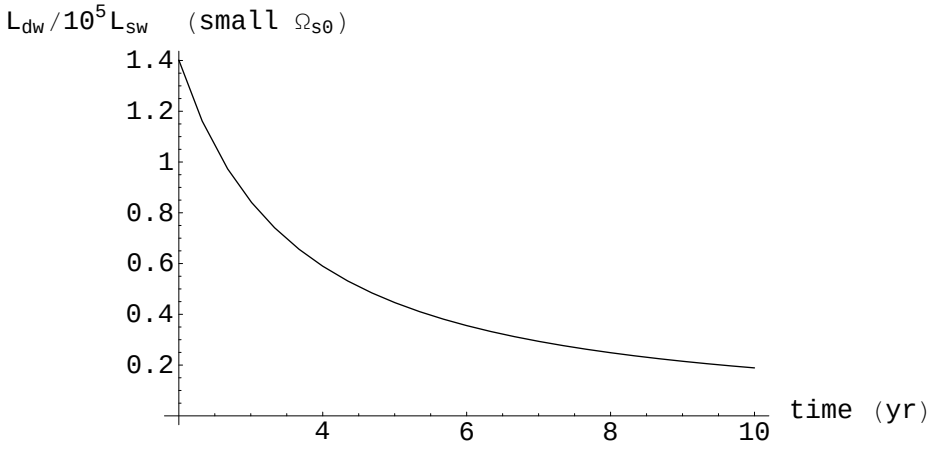
$L_{dw}/10^5 L_{sw}$ (small Ω_{s0})
1.4
1.2
1
0.8
0.6
0.4
0.2
4
6
8
10
time (yr)

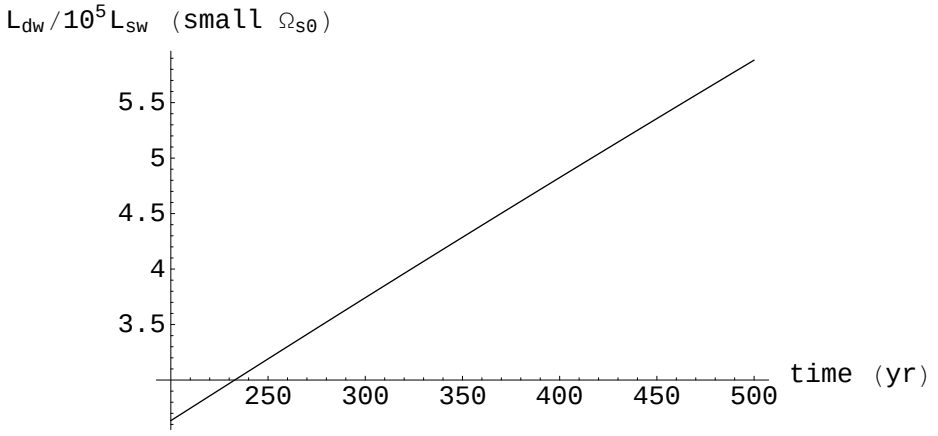
$L_{dw}/10^5 L_{sw}$ (small Ω_{s0})
5.5
5
4.5
4
3.5
250
300
350
400
450
500
time (yr)

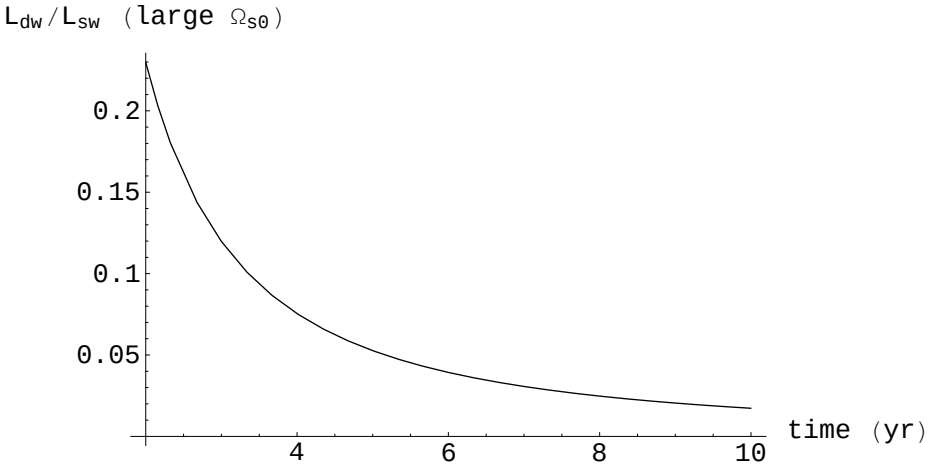
L_{dw}/L_{sw} (large Ω_{s0})
0.2
0.15
0.1
0.05
4
6
8
10
time (yr)

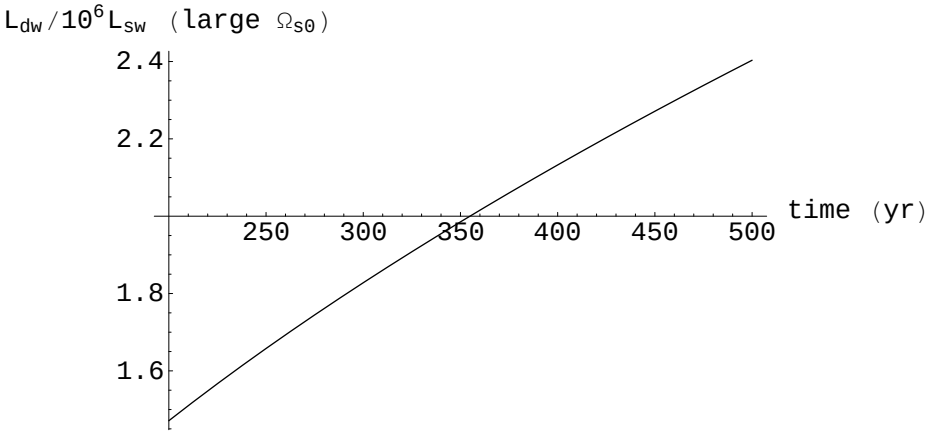
$L_{dw}/10^6 L_{sw}$ (large Ω_{s0})
2.4
2.2
1.8
1.6
250
300
350
400
450
500
time (yr)

This figure "Fig2all.jpg" is available in "jpg" format from:

http://arXiv.org/ps/astro-ph/0005288v3